AGU PUBLICATIONS

JGR

Journal of Geophysical Research: Solid Earth

RESEARCH ARTICLE
10.1002/2014JB011514

Key Points:
- A new interpretation of landslide-induced tsunamis at Valdez, Alaska
- Numerical models match observations of tsunami height and current direction
- We image slide pathways and deposits

Correspondence to:
T. Parsons,
tparsons@usgs.gov

Citation:
Parsons, T., E. L. Geist, H. F. Ryan, H. J. Lee, P. J. Haeussler, P. Lynett, P. E. Hart, R. Sliter, and E. Roland (2014), Source and progression of a submarine landslide and tsunami: The 1964 Great Alaska earthquake at Valdez, *J. Geophys. Res. Solid Earth*, *119*, 8502–8516, doi:10.1002/2014JB011514.

Received 1 AUG 2014
Accepted 17 OCT 2014
Accepted article online 22 OCT 2014
Published online 16 NOV 2014

Source and progression of a submarine landslide and tsunami: The 1964 Great Alaska earthquake at Valdez

Tom Parsons[1], Eric L. Geist[1], Holly F. Ryan[1], Homa J. Lee[1], Peter J. Haeussler[2], Patrick Lynett[3], Patrick E. Hart[1], Ray Sliter[1], and Emily Roland[2,4]

[1]U.S. Geological Survey, Menlo Park, California, USA, [2]U.S. Geological Survey, Anchorage, Alaska, USA, [3]Department of Civil and Environmental Engineering, University of Southern California, Los Angeles, California, USA, [4]School of Oceanography, University of Washington, Seattle, Washington, USA

Abstract Like many subduction zone earthquakes, the deadliest aspects of the 1964 $M = 9.2$ Alaska earthquake were the tsunamis it caused. The worst of these were generated by local submarine landslides induced by the earthquake. These caused high runups, engulfing several coastal towns in Prince William Sound. In this paper, we study one of these cases in detail, the Port Valdez submarine landslide and tsunami. We combine eyewitness reports, preserved film, and careful posttsunami surveys with new geophysical data to inform numerical models for landslide tsunami generation. We review the series of events as recorded at Valdez old town and then determine the corresponding subsurface events that led to the tsunami. We build digital elevation models of part of the pretsunami and posttsunami fjord-head delta. Comparing them reveals a ~1500 m long region that receded 150 m to the east, which we interpret as the primary delta landslide source. Multibeam imagery and high-resolution seismic reflection data identify a ~400 m wide chute with hummocky deposits at its terminus, which may define the primary slide path. Using these elements we run hydrodynamic models of the landslide-driven tsunamis that match observations of current direction, maximum inundation, and wave height at Valdez old town. We speculate that failure conditions at the delta front may have been influenced by manmade changes in drainage patterns as well as the fast retreat of Valdez and other glaciers during the past century.

1. Introduction

At 5:36 P.M., on 27 March 1964, one of the largest earthquakes of the twentieth century struck beneath Alaska's Prince William Sound. The $M = 9.2$ earthquake ultimately killed 131 people, most of whom perished because of the tsunamis it caused, some as far away as California. More people were killed at Valdez (33) than at any other locale because part of the fjord-head delta front collapsed adjacent to the town of Valdez. The town was engulfed almost immediately by the resulting tsunami. Valdez old town was originally located on the east end of the east-west trending Port Valdez fjord (Figure 1), which is Alaska's northernmost ice-free port, and current terminus of the Trans-Alaskan Pipeline System. The site at Valdez old town was deemed too unsafe for rebuilding due to the potential for future failures. The town was moved to its present location on the north side of the fjord, and a moratorium established on building at the old town site that expired in 2014 (Figure 1).

In this paper we present new seismic reflection data, bathymetric differencing, and numerical modeling of the landslide-generated tsunamis that affected the town of Valdez to unravel the subsea slide events of 27 March 1964. The occurrences above sea level at Valdez are well documented by film, eyewitnesses, and postearthquake technical assessments. Additionally, many features of the landslide that are preserved underwater allow us to piece together what happened. As virtually every coastline in the world is vulnerable to landslide-induced tsunamis, a detailed portrait of the subsea process provides an observational benchmark in terms of the scale of wave heights that might be expected for this slide volume and geometry.

2. Observations

2.1. Sequence of Events at Valdez Old Town Above Water Level

On the afternoon of 27 March 1964, the ~400 ft (120 m) Alaskan Steamship Company vessel *S.S. Chena* was tied up at the north dock at Valdez. Its arrival was a twice per year event for the town as fresh supplies

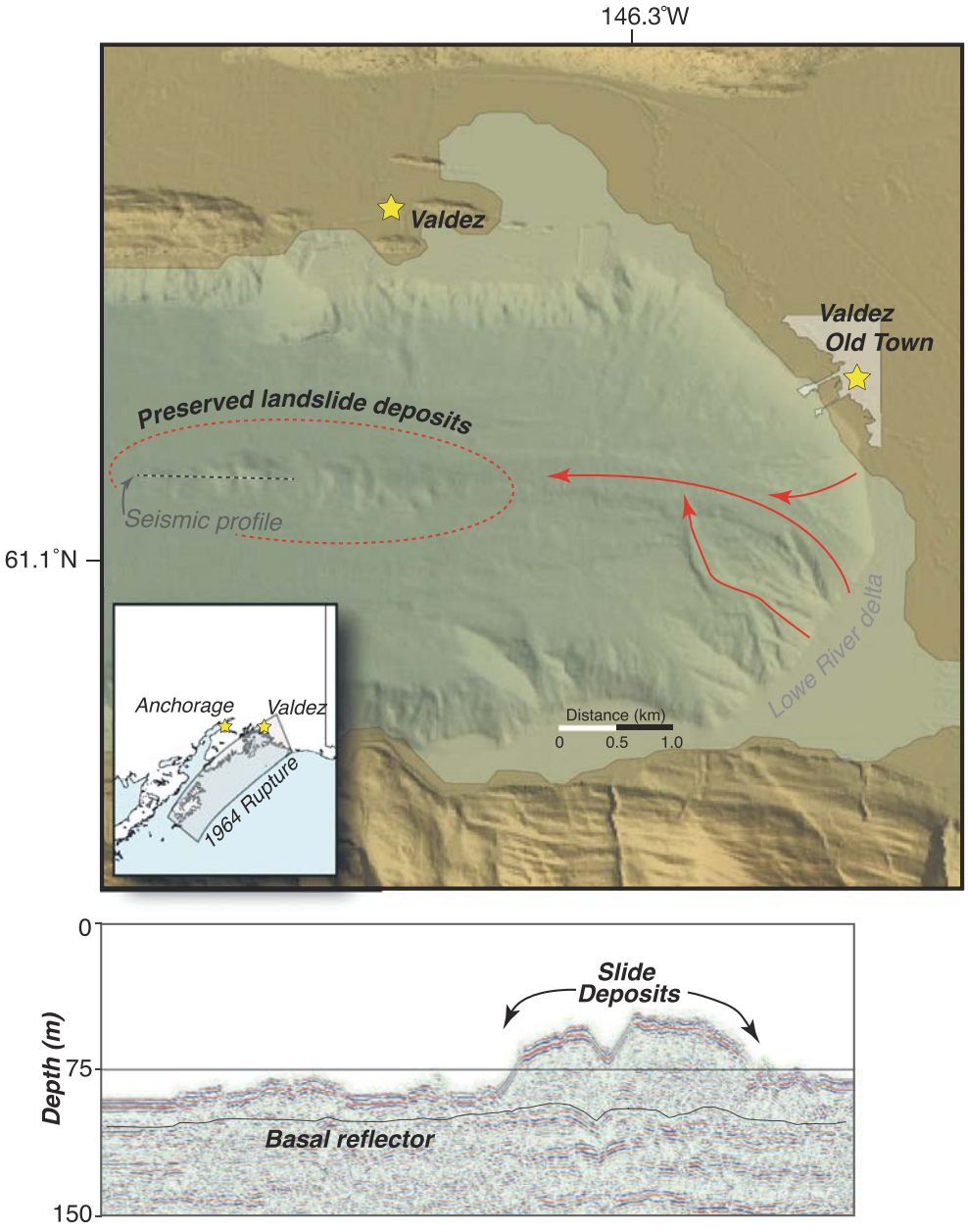

Figure 1. (top) Merged bathymetry and topography on the east end of Port Valdez. The 1964 Alaska earthquake caused submarine landslides at the fjord margin, inundating Valdez old town. Preserved landslide deposits are evident on the fjord bottom at ~300 m depth. Likely slide paths are marked by red arrows. Valdez town was moved to its present location to the northwest after the 1964 tragedy. A multichannel sparker reflection profile (bottom) across landslide deposits aids in their interpretation because a continuous basal reflector can be seen beneath them, which is strongly suggestive of a recent translational origin.

were being delivered, and many residents, including young people, were on the docks to greet it. Two crew members happened to have been filming with handheld cameras, and their footage provides the primary direct evidence of the 1964 earthquake effects at Valdez. Unfortunately, the film (Source: *Alaska Film Archives*: http://library.uaf.edu/film-archives) was cut and spliced in incorrect order shortly after the earthquake, meaning the exact sequence of events is still somewhat uncertain, and depends on a number of eyewitness accounts from the town and from the *Chena*. We provide a timeline here that focuses on the behavior of the sea, and that is based on the interviews, analyses, and summaries by *Brown* [1964], *Coulter and Migliaccio*

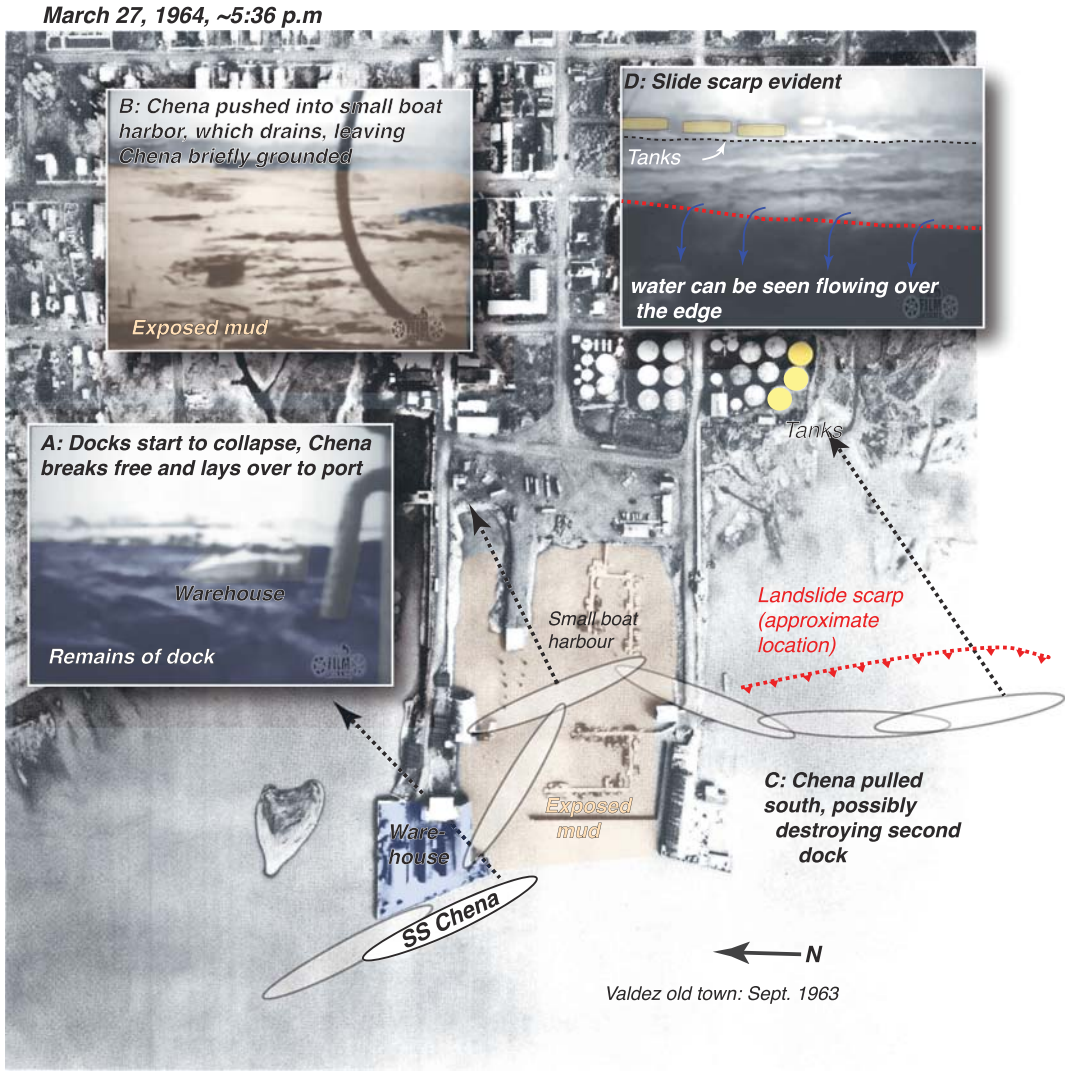

Figure 2. Sequence of events during the initial stages of the Valdez tsunami. Images are stills from movies taken by *S.S. Chena* crewmen (courtesy of the University of Alaska Film Archives and Bartlett Collection) superposed on an air photo. Dashed arrows show the approximate view directions from the *Chena* for each still, and the primarily southward drift of the vessel resulting from cyclical drawdown and flooding is shown. (a) Witnesses in town noted that the *Chena* nearly disappeared from view as docks collapsed; the vessel subsequently was pulled away from the docks to the northwest before almost immediately being pushed back onto the dock and into the small boat harbor. (b) The exposed harbor floor can be seen, as water is slow to refill it. (c) The *Chena* is drawn southeast through the south dock by a strong current. (d) Water can be seen cascading over the north extent of the landslide scarp.

[1966], and *Wilson and Tørum* [1971] (Figure 2). Many (if not most) accounts of the earthquake and tsunami focus on the extraordinary movements of the *Chena*.

Very shortly after the initial shock was felt on land and at sea, several things are said to have occurred almost simultaneously: (1) the first movement of the *Chena* was the ship's being pulled away from the collapsing docks to the northwest, (2) the collapsed docks were still visible (Figure 2a) but ruined (meaning they were not taken out by a submarine landslide, as was initially thought) [e.g., *Coulter and Migliaccio*, 1966], (3) the *Chena* laid over to port by at least 50°, and (4) a strong drawdown of the sea left the bay floor exposed in the small boat harbor (Figure 2b).

About a minute later the *Chena* is said to have risen ~6 to 9 m on an incoming wave; this is reported from the town and the ship. The sight of this large vessel being tossed about seems to have been the primary focus of most witnesses in town. Tragically, the *Chena* then slammed down on the docks where many people

were congregated, and most of the casualties in Valdez happened at this point. This image haunted all who saw it. The *Chena* then washed aground into the small boat harbor, which was filling slowly because of damming by the two jetties connecting the north and south piers to town (Figure 2). The *Chena*'s stern was at that point dug into the bay mud, and the vessel tried to regain power, but could not turn. Continued return flow freed the *Chena*, which regained power and tried to move out to sea, but could not because of extremely strong alongshore currents that pulled the ship across the south docks and southeast along the shore. From this vantage, crew members were able to film water cascading over the north edge of the submarine landslide scarp (Figure 2d). The *Chena* ultimately escaped to deeper water and, remarkably, was left undamaged. Unfortunately, the same cannot be said about Valdez old town.

There are numerous and sometimes conflicting accounts about the initial wave height at Valdez old town; the most direct accounts come from *Brown* [1964], who spoke to eyewitnesses and concluded, "Almost instantaneously, the Valdez dock broke and collapsed into the water. This was followed by a great destructive surge of water some 15 to 25 ft high (4.5 to 7.6 m), though some reports indicate it to be as much as 30 to 40 ft (9 to 12 m). Following this activity the water subsided to approximately half-tide level." Complicating the estimates of water height are effects of subsidence at Valdez old town, estimated to be about 2.7 m on the waterfront, based on highway profile surveys, and 3 m at the dock gate [*Coulter and Migliaccio*, 1966]. By all accounts, a second, smaller wave struck the town about 10 min after the first. Water from this wave is reported to have reached a depth of ~0.5 m in the Valdez Hotel on McKinley Street (one block inland from the harbor) [*Coulter and Migliaccio*, 1966], as compared with ~4.5 m at the same site from the initial wave [*Wilson and Tørum*, 1971]. Maximum inundation in Valdez old town extended ~550 m from shore, up to elevations of 4.9 to 5.5 m above sea level (postearthquake contours) [*Wilson and Tørum*, 1971].

2.2. Sequence of Events Near Valdez Old Town Below Water Level

There was little doubt about the cause of the tsunamis at old town Valdez, even as they were happening. Failure of the Valdez delta front occurred during earthquakes in 1899, 1908, 1911, 1912, and 1925, [*Coulter and Migliaccio*, 1966] though clearly not to the degree that it did in 1964. A complicating factor at Valdez was the construction of a dike and levee system around the town that diverted virtually all the drainage to the south of the town since the 1930s [*Coulter and Migliaccio*, 1966], and that may have contributed to an unstable sediment buildup on the delta front there. Additionally, Valdez Glacier has been melting at fairly high rates, receding about 950 m between 1901 and 1964 and a cumulative 2.6 km between 1901 and 2008 [*World Glacier Monitoring Service*, 2008]. The glacier loses about 0.22 km^2 in area each year, and it has thinned significantly [*Arendt et al*., 2006]. The accompanying unweighting, reduced normal stress, and increased focused sedimentation [*Barclay et al*., 2009] likely contributed to the instability of the delta front south of the town. The Lowe River drains a large area containing several other receding glaciers and feeds the delta farther south of Valdez old town as well.

Here we reconstruct the location and shape of the source region for the submarine landslides on the delta front based on multibeam bathymetry and subbottom seismic reflection profiling. To identify the primary failure source areas, we create and compare digital elevation models (DEMs) made from a preearthquake bathymetric survey conducted in 1959 [*Seaborg*, 1959] and a postearthquake multibeam survey completed by the National Oceanic and Atmospheric Administration (NOAA) in 2006 [*Caldwell et al*., 2011].

A hydrographic survey was concentrated on the region around Valdez harbor in 1959, using a lead line and a fathometer mounted to a small, shallow-draft skiff to get 993 single-point measures of depth at variable spacing [*Seaborg*, 1959] (Figure 3). Third-order triangulation control was established to benchmarks onshore and to hydrographic markers on the horizontal North American Datum of 1927 (NAD27). We digitized depth points on this projection, converted them from fathoms to meters, added 3.32 m to the original values to reference them to mean higher high water [*Seaborg*, 1959], and then converted point locations to the NAD83 horizontal datum using NOAA NADCON software. For the postearthquake DEM we use 3-D points from the multibeam bathymetry surveys in Prince William Sound completed by NOAA in 2006 [*Caldwell et al*., 2011], with a vertical datum at mean higher high water. The horizontal datum is set to the World Geodetic System datum of 1984 (WGS84); the horizontal difference between NAD83 and WGS84 is approximately 1 m across North America, which is significantly less than the minimum point spacing of the multibeam survey (15 m).

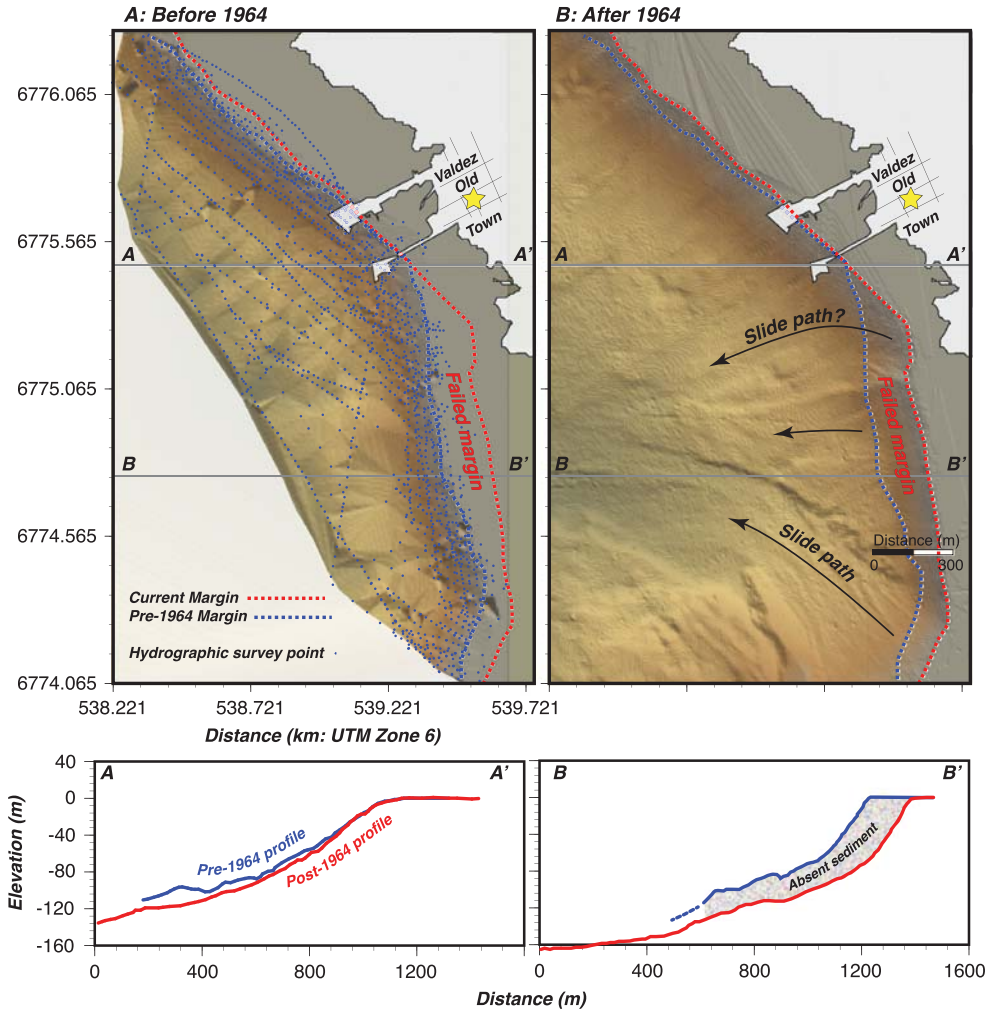

Figure 3. (a) A hydrographic survey conducted in 1957 gives the approximate preearthquake shape of the fjord margin near Valdez old town and the location of the slope edge. (b) Multibeam bathymetry data show the postlandslide configuration, with parts of the slope edge recessed ~150 m east of the preearthquake location, mostly south of Valdez old town (labeled "Failed margin"). Cross sections A-A' and B-B' show differences between the two surveys where the margin is largely unchanged and where significant submarine landsliding took place, respectively.

Comparison of the DEMs corresponding to the 3-D point data obtained from the preearthquake and postearthquake bathymetric surveys shows that a significant part of the Valdez delta is missing (Figure 3) and presumably failed during the 1964 earthquake. Along a ~1500 m long zone, the delta front moved about 150 m eastward. It is clear that the primary delta failure within this area occurred south of Valdez old town, and not directly adjacent to the harbor as concluded by *Coulter and Migliaccio* [1966], although some failure did occur at the harbor as observed by scuba divers shortly after the earthquake, where portions of the harbor are up to 20 m deeper [*Grantz et al.*, 1964]. *Nicolsky et al.* [2013] also concluded that most of the slide source was south of Valdez old town. The northernmost reach of the landslide scarp we interpret in Figure 3 is consistent with the location of the one filmed on board the *Chena* (Figure 2d). Finally, the location of the primary landslide south of Valdez old town is also consistent with the redirected drainage, and assumed delta buildup to the south of the town after the 1930s dike and levee system was in place.

We find, based on the changes in bathymetry before and after the 1964 earthquake, that submarine landslides initiated on the oversteepened delta front south of Valdez old town. We note from the multibeam bathymetry that there are three channels that all emerge from this zone and coalesce into a 400 m wide primary channel downslope (Figures 1 and 3). Such linear slope "chutes" have been associated with submarine landslides in many other locations [e.g., *Twichell et al.*, 2009; *Tappin*, 2010; *Migeon et al.*, 2011;

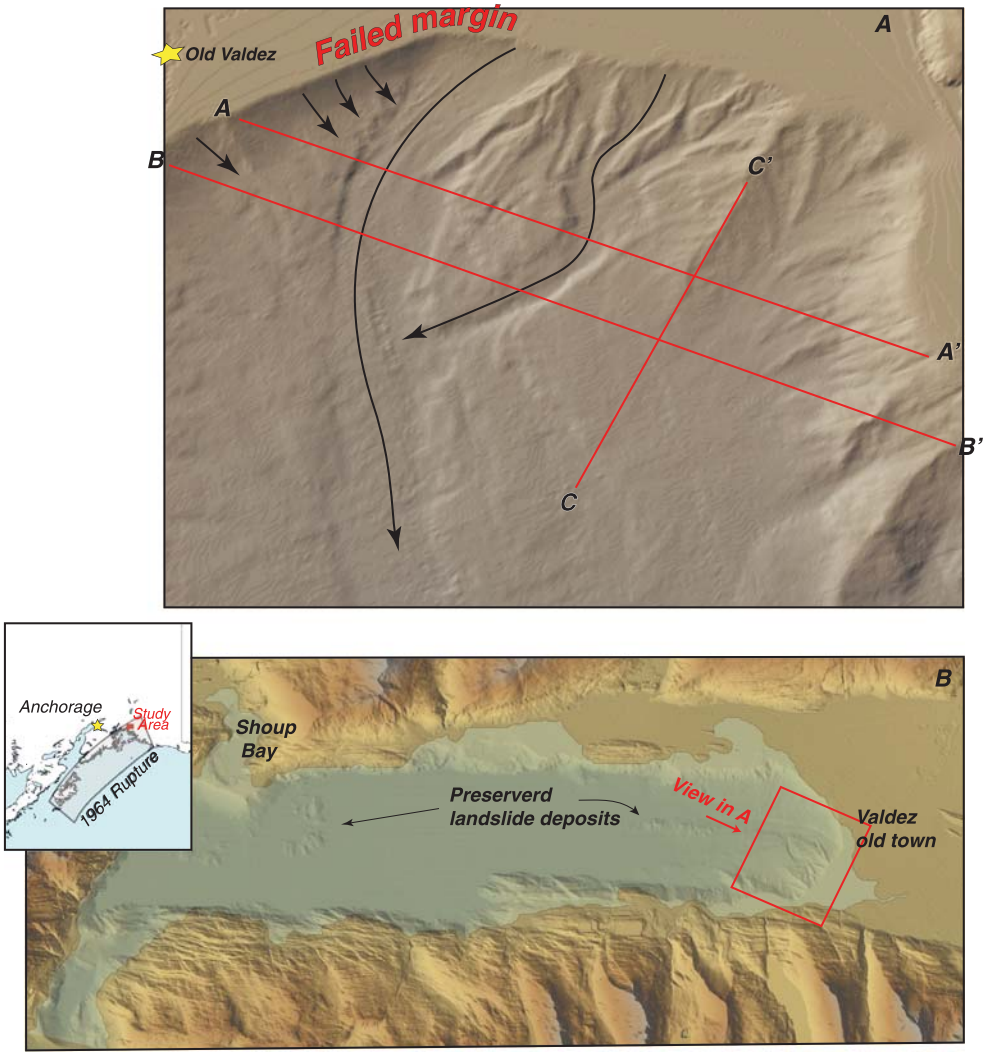

Figure 4. (a) A 3-D perspective view from the multibeam DEM with seismic profile locations and (b) the whole fjord bathymetry is shown, including landslide deposits from both the delta-front failures and Shoup Bay moraine.

Jintasaeraneea et al., 2012; *Dalla Valle et al*., 2013; *Gales et al*., 2014; *Laberg et al*., 2014]. These are the primary pathways that landslide materials moved downslope on the Valdez delta front; we conclude this from interpreting the combination of multibeam bathymetry and subbottom seismic reflection profiling. These slide paths may have exploited preexisting channels from turbidity currents generated by hyperpycnal flows out of the Lowe River or Valdez glacier drainage or smaller earlier debris flows.

Multibeam bathymetry has been used previously to identify preserved landslide deposits on the Port Valdez fjord floor [*Lee et al*., 2006, 2007; *Ryan et al*., 2010], including those evident at the ends of submarine slide channels shown in Figure 1. Multichannel seismic reflection profiles show that these deposits are lying on top of the prior seafloor and are underlain by continuous reflection horizons (Figure 1). Additional deposits can be seen on the west end of the fjord (Figure 4), adjacent to the Shoup Bay moraine, and are interpreted as separate failures from those at Valdez old town [*Lee et al*., 2006, 2007; *Ryan et al*., 2010]. Also, three large debris lobes have been mapped on the floor of the fjord west of the area shown in Figure 1 [*Lee et al*., 2007]. These contain sandy material and the overlying sediment has been dated using Cs^{137} techniques showing that the debris lobes correspond to the 1964 event.

To gain a better, more detailed understanding of the submarine landslide processes at the fjord-head delta, the U.S. Geological Survey collected a densely spaced (100–500 m apart) grid of high-resolution seismic

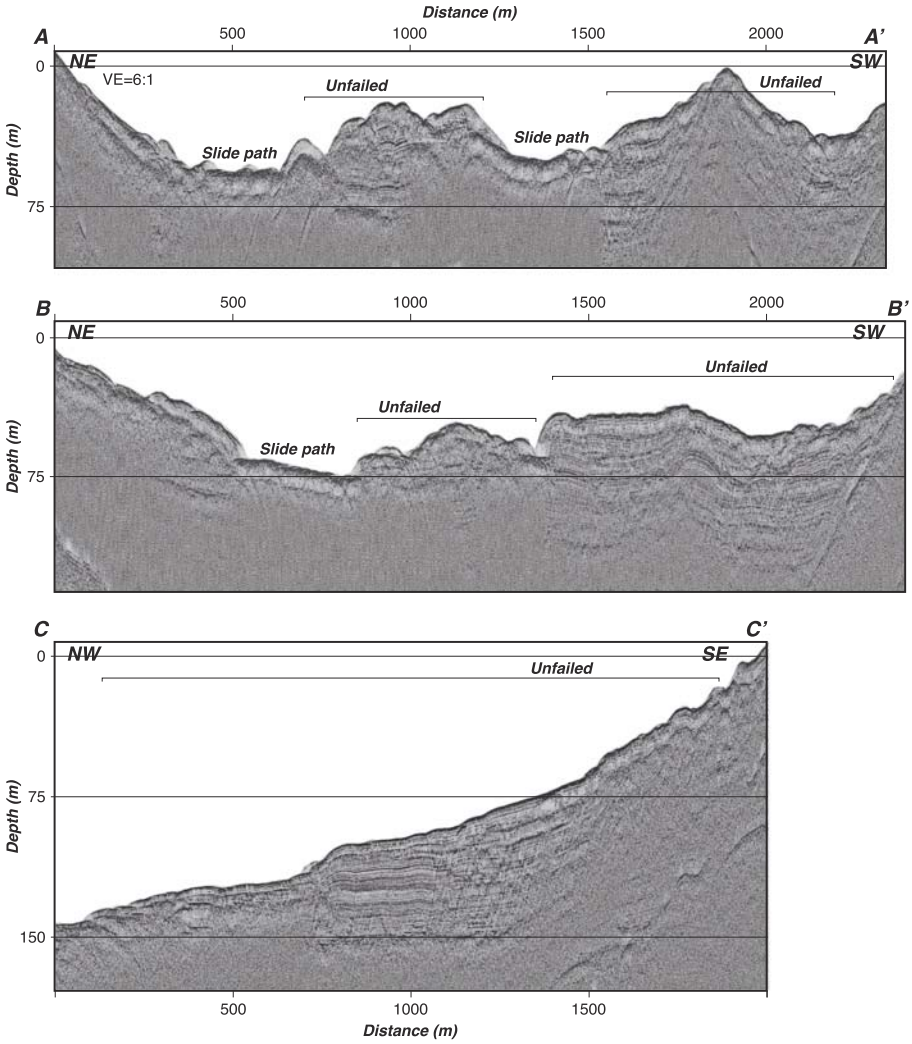

Figure 5. (a) Seismic reflection profile A-A′ recorded from a chirp source. It shows mostly unfailed sediment accumulation (~75 m thick) on the delta front but crosses two landslide channels labeled "slide path." (b) The cross-section B-B′ is shown from a little further downslope. (c) An orthogonal view shows the continuity of sedimentary deposits. Profile locations are shown in Figure 4.

reflection profiles across the eastern end of Port Valdez in September of 2013. The profiles were collected with a chirp subbottom profiling system using a 500–7200 Hz swept frequency source pulse that can resolve vertical layering as thin as ~0.25 m and can penetrate to ~100 m subbottom depths, depending on recording conditions. Multiple profiles that crossed the delta front show continuous layering typically down to 75–80 m, and that show no interruptions throughout the sections. Example profiles are shown in Figure 5, where sediment appears to have been deposited on an uneven substrate, and that shape is mirrored through the entire section, from deepest observed to the surface. There are cuts through these sections that correspond to two submarine channels interpreted from the multibeam bathymetry; these paths have comparatively hard surfaces such that the chirp source cannot penetrate through them (Figure 5). These channels provide likely landslide pathways that lead to deposition sites.

We conclude that the sequence of subsea events at the delta front during the 1964 earthquake occurred as (1) a ~1500 m wide zone collapsed south of Valdez old town, and then (2) coalesced into, and flowed downslope in, a ~400 m wide erosional channel, with part of the material coming to rest as (3) a chain of hummocky deposits on the fjord floor (Figure 1). Mobilized sandy sediment continued as a debris flow past the hummocky deposits, forming part of the massive lobe of sediment, which covers the eastern three

fourths of the deep floor of the fjord [*Lee et al*., 2007; *Ryan et al*., 2010]. This sudden change in the shape of the seafloor near the source region displaced a significant amount of water that caused the deadly tsunami that struck Valdez old town shortly afterward.

We cannot rule out the occurrence of additional debris flows during the 1964 earthquake; indeed hundreds of individual subaerial and submarine landslides were observed during a 2007 $M = 6.1$ earthquake in an example from a Chilean fjord [*Lastras et al*., 2013]. Further, *Nicolsky et al*. [2013] are able to reproduce observed runup at Valdez old town with a far-traveled debris flow model. Here we investigate whether the simplest landslide scenarios can explain the observations; establishing the range of possible model fits is useful since quantitative landslide tsunami forecasts are becoming more prevalent [e.g., *Masson et al*., 2006; *ten Brink et al*., 2009; *Suleimani et al*., 2011; *Nicolsky et al*., 2013].

3. Tsunami Generation

We test a hypothesis that the most damaging tsunami events at Valdez old town resulted from the submarine landslide scenario we interpret from multibeam and seismic reflection imaging on the east end of Port Valdez (Figure 3) and previous work in the western part of Port Valdez [*Lee et al*., 2007; *Ryan et al*., 2010]. To do this, we model tsunamis as resulting from two submarine landslide sources: (1) a primary failure of a ~1500 m wide zone along the delta front just south of Valdez old town that funneled into a 400 m wide chute and (2) a secondary failure source of the moraine near the outlet of Shoup Bay [*Lee et al*., 2007; *Ryan et al*., 2010].

3.1. Tsunami Modeling Methods

Two primary categories of submarine landslide deposits are observed from the 1964 earthquake in Port Valdez fjord: (1) long-traveled, sandy debris flows that are broadly distributed and (2) short-traveled hummocky (and/or possibly blocky) deposits (Figure 1) [*Lee et al*., 2007]. Our hypothesis is that the preserved hummocky deposits observed at the end of the narrow chutes on the fjord-head delta slid down those chutes and were the primary cause of the tsunami at Valdez old town. We suspect this to be the case because the continuity and proximity of the deposits would enable significant and rapid tsunami generation. We conduct numerical modeling to determine how many of the observations at Valdez old town can be explained with this scenario.

A number of landslide tsunami modeling approaches exist that include rigid-block movement and viscous and granular flows on a slope [e.g., *Jiang and Leblond*, 1994; *Ward*, 2001; *Fernández-Nieto et al*., 2008]. Alternatively, kinematic forcing functions that combine rotational and translation motion [*Lynett and Liu*, 2002, 2005] can realistically emulate the mapped geometry of excavation and deposition regions associated with landslides. We find that the observed deposits at Port Valdez are best described as either debris flows, or debris avalanches that may have entrained blocky material. That they lie at the termination of chutes suggests that these flows excavated as they moved downslope. We cannot discern any internal structure within the deposits [*Lee et al*., 2007; *Ryan et al*., 2010] (Figure 1), and thus do not know how contiguous they might be. We therefore want to apply modeling techniques that can estimate the expected rheology of the flows and that can model effects of downward movement in the excavation region and upward movement in the deposition region in two horizontal dimensions. This roughly emulates a debris flow or debris avalanche. As we are uncertain about the time history of the flows, we approximate them as a viscoplastic material that behaves quasi-rigidly at low stresses but flows as a viscous fluid at high stress. This enables simulation of a range of possible apparent yield stresses and can represent fluid and quasi-rigid behavior that informs the time history of tsunami-generating functions. Below we describe the specific numerical techniques that we apply for debris-flow and tsunami modeling.

3.1.1. Debris-Flow Viscoplastic Model

We use the BING model developed by *Imran et al*. [2001] to calculate the time history of the observed slides on the Valdez delta front (highlighted in Figure 4). BING is a 1-D numerical model of a viscoplastic fluid flowing over an arbitrary slope in either a subaerial or subaqueous environment. Various rheologies can be specified in BING, including Bingham plastic, nonlinear Herschel-Bulkley, and *Locat*'s [1997] bilinear rheology, the latter of which we use to model the Valdez debris flows. The bilinear rheology was originally intended for clayey silt and silt mixtures and assumes that flow at low-strain rates is Newtonian, whereas at high-strain rates the flow exhibits Bingham behavior. The dimensions of the initial failure shape and final deposit interpreted from bathymetric profiles are used to estimate the rheological parameters in BING

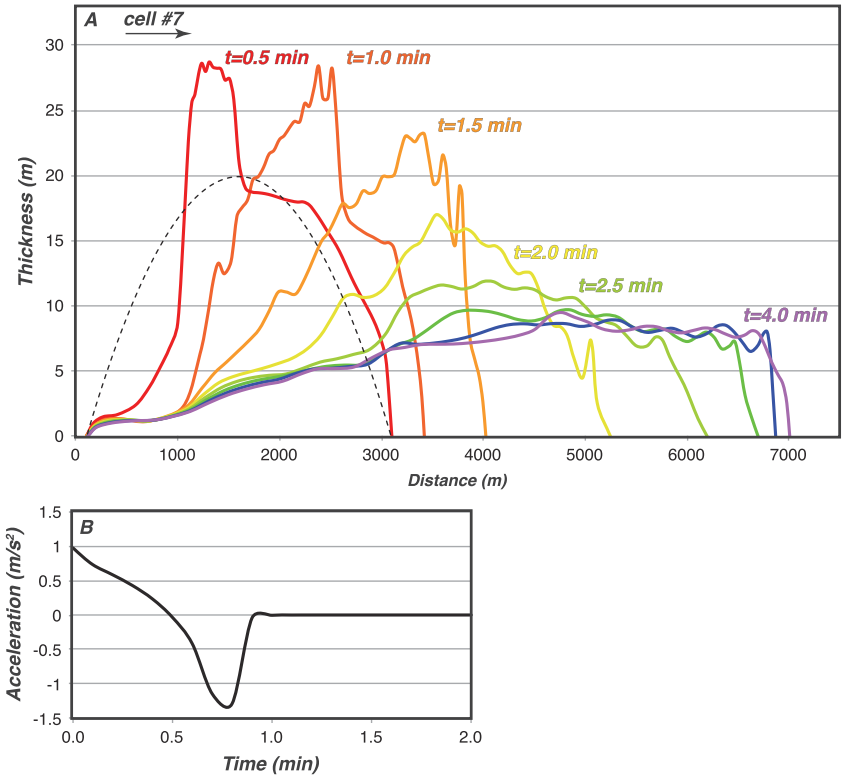

Figure 6. Results from BING modeling of drebis flow. (a) Thickness profiles for the first 4 min of movement are shown at 0.5 min increments. The initial thickness profile is parabolic, as indicated by the black dashed line. (b) The acceleration time history for cell #7 is shown, which is located 420 m from the back of the slide. The horizontal downslope movement of cell #7 is indicated by the arrow in Figure 6a.

by iteration, similar to analysis of the Palos Verdes debris avalanche offshore southern California [*Locat et al.*, 2004] and the Currituck slide offshore of North Carolina [*Locat et al.*, 2009]. The preslide and postslide bathymetry and topography are reasonably well defined for the easternmost part of the fjord (Figures 3 and 4). We use the bathymetric profile along the slide path, including the preserved hummocky deposits as the postslide change, and compare that with the adjacent, unfailed slope as the preslide profile. We neglect the debris lobes that may have bypassed the hummocky deposits and continued west into the deeper parts of the fjord. Of the different parameters associated with the bilinear rheology, apparent yield strength of the Bingham phase of flow is the primary parameter that controls the end shape of the slide for a given geometry and volume.

The BING modeling using before-and-after bathymetric profiles finds their geometry to be most consistent with an apparent yield strength of 6500 Pa. This value is associated with the hummocky deposits we observe and does not reflect the lower yield stress that would have determined where all of the debris flow stopped. Similar modeling results were found for the Palos Verdes slide (5000 Pa) [*Locat et al.*, 2004] and the Currituck slide (2000 Pa) [*Locat et al.*, 2009]. Much lower yield strengths (5 to 10 Pa) are calculated for far-reaching debris flows [*Schwab et al.*, 1996], and our modeling finds order of magnitude lower values to fit the long-traveled lobes observed in western Port Valdez by *Lee et al.* [2007] and *Ryan et al.* [2010].

The time history of the Valdez delta-front slide is shown in Figure 6a. The time history of the slide is complex, owing to the sharp change of slope in the fjord combined with the bilinear rheology. There is rapid downward movement in the excavation region, starting at the back of the slide and progressing down the steep slope of the fjord. During the first minute after failure, a pulse of sediment moves downslope through the excavation region. Then, the flow moves across the lower slope floor of the fjord at slower rates compared to the initial movement at the back of the slide. In terms of tsunami generation, *Enet and Grilli* [2007] indicate that for rigid landslides, acceleration is the principal factor that controls the amplitude

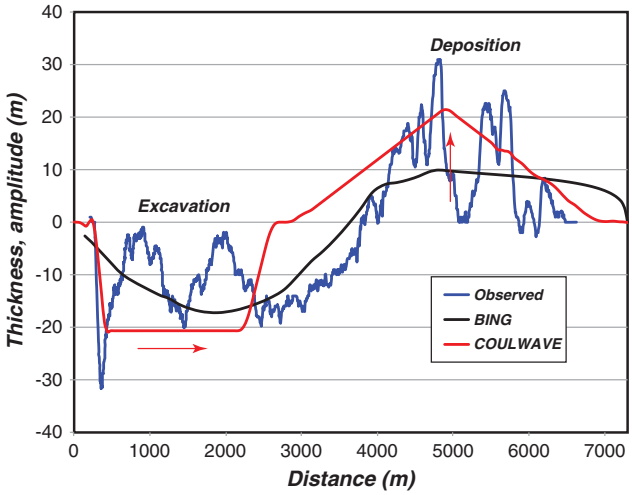

Figure 7. Comparison of three downslope profiles. The blue line shows the observed bathymetric difference profile along the axis of the chute deposits shown in Figure 1. The black shows results from the BING model after 10 min; the initial parabolic mass is shown by negative values to compare with the excavation region. The red line shows the final profile of the time-varying tsunami-generating function used by COULWAVE at the water surface. Arrows indicate the primary horizontal and vertical temporal variations used in COULWAVE.

of the generated tsunami. The acceleration/deceleration phase of movement in the excavation region occurs within approximately 1 min, according to the BING model (Figure 6b). We use this time for modeling tsunami generation in the hydrodynamic model.

3.1.2. Tsunami Hydrodynamic Model

The modeling method used for this study is the Cornell University Long and Intermediate Wave Modeling package (COULWAVE) [*Lynett and Liu*, 2002]. COULWAVE was developed to model the propagation and runup of long- and intermediate-length waves, using a range of different wave theories, including fully nonlinear and dispersive wave equations (i.e., the nonlinear Boussinesq equations) as described by *Lynett and Liu* [2002], *Lynett et al.* [2002], *Lynett and Liu* [2005], and *Lynett* [2006]. For this study, we use the fully nonlinear and nondispersive wave equations [*Lynett and Liu*, 2002], i.e., the nonlinear shallow-water wave equations. The dominant period of the wave near the source region is approximately 2 min such that the generated tsunami is well within the longwave regime. Additionally, higher harmonics with periods approaching 30 s are generated through nonlinear processes in shallow (~10 m) water depths. These wave frequency and depth combinations are well described by nondispersive wave theory. COULWAVE also uses a moving boundary condition to emulate onshore flow and inundation associated with the tsunami.

Numerical models of landslide tsunamis such as COULWAVE require several parameters as input. The volume and shape of the slide are defined by the preslide and postslide bathymetry, also used in the debris-flow model described in section 3.1.1. The results of the debris-flow model provides information on the time history of the slide, in particular the primary phase of tsunami generation (Figure 6). The propagation and runup computations are based on regional bathymetry and topography for which we created a 40 m gridded DEM. Bottom friction (f) accounts for turbulent flow along the ocean floor and is parameterized in COULWAVE such that shear stress (τ) at the bottom boundary is given by

$$\tau = \frac{1}{2}\rho f |\mathbf{u}_b| \mathbf{u}_b,$$

where ρ is fluid density and $\mathbf{u}_b$ is the horizontal velocity field near the seafloor. Lastly, wave breaking is implemented in COULWAVE using the eddy viscosity model of *Kennedy et al.* [2000] with modifications described by *Lynett* [2006]. The results of preliminary sensitivity tests on parameters needed to run COULWAVE (e.g., linear versus nonlinear equations, bottom friction, and energy dissipation from wave breaking) suggest that bottom friction and linear versus nonlinear formulation have the greatest effect on the results [e.g., *Geist et al.*, 2009]. We test a range of bottom friction values from $f = 0.01$ to $f = 0.001$ that is considered reasonable for submarine conditions [*Park et al.*, 2013], though this parameter range produces variation in maximum wave height of less than 1 m for this case.

The landslide source for tsunami waves is described by its geometry and duration of vertical displacement in the excavation and deposition regions. The landslide geometry is specified by lengths and depths of the erosional and depositional zones and the slide width. Smooth, temporally varying functions are used in COULWAVE to specify tsunami generation from landslides [*Lynett and Liu*, 2001, 2002, 2005]. These functions balance a realistic description of geologic processes with numerical stability required to solve the

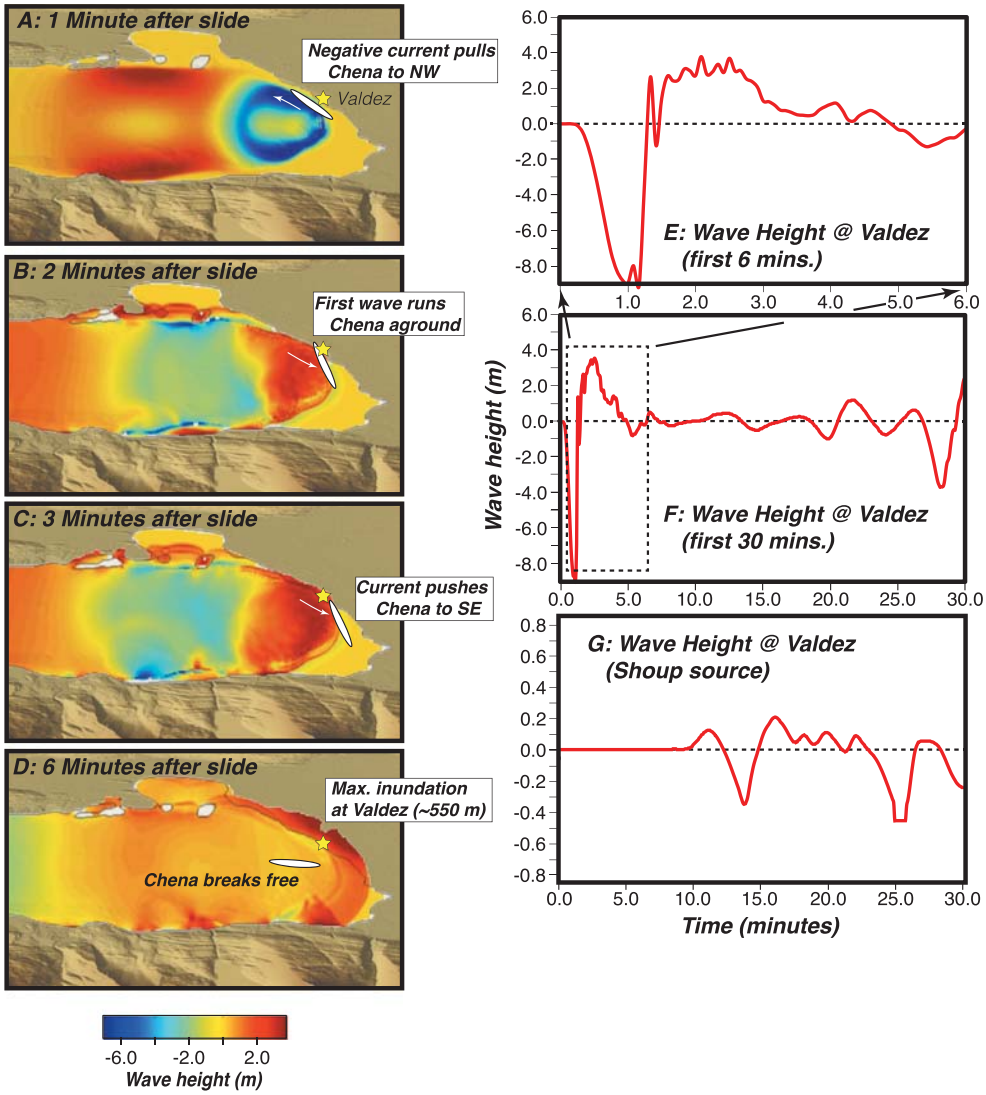

Figure 8. Results of hydrodynamic modeling of the Valdez delta-front landslide geometry as defined in this paper. (a) The primary negative pulse is shown that drained Valdez harbor and pulled the *S.S. Chena* off its moorings. (b) The large positive phase quickly overcomes the negative pulse. The wave propagates eastward, generating (c) the alongshore current that trapped the *Chena* (Figure 2). (d) The maximum inundation in Valdez occurs, reaching about 500 m inland and closely matching the observations cataloged by *Wilson and Tørum* [1971]. (e) The time series of wave height (marigram) is plotted at a point just offshore of Valdez old town covering the initial 6 min. The maximum water height on land is about 4.5 m, close to the low estimate of wave height from eyewitness accounts of 4.6 m. (f) The same information is shown except for a 30 min period. For comparison, in Figure 8g, a marigram is shown based on a model of the landslides that occurred near Shoup Bay (see Figure 4 for location).

hydrodynamic equations. Smooth forcing functions for sea surface elevations are also physically reasonable because small-scale changes in seafloor displacement are attenuated through the water column. These functions include both translational and rotational type motions. As shown in Figure 7, the excavation region is modeled as a 20 m negative amplitude pulse that rapidly progresses downslope during the first minute, whereas the depositional region is modeled by a positive amplitude pulse that increases with time such that the excavation and deposition volumes are conserved. While the source width for the Valdez delta-front slide is at least 1500 m, it eventually becomes partially channeled into a single, 400 m wide chute (Figures 1 and 3). We treat the slide as a single 400 m wide zone, which likely minimizes its volume. In COULWAVE, a smooth Gaussian function is used to model the cross-slope profile of the slide, such that the width is defined as the separation between locations where the Gaussian function is 1% of its maximum [*Lynett and Liu*, 2005].

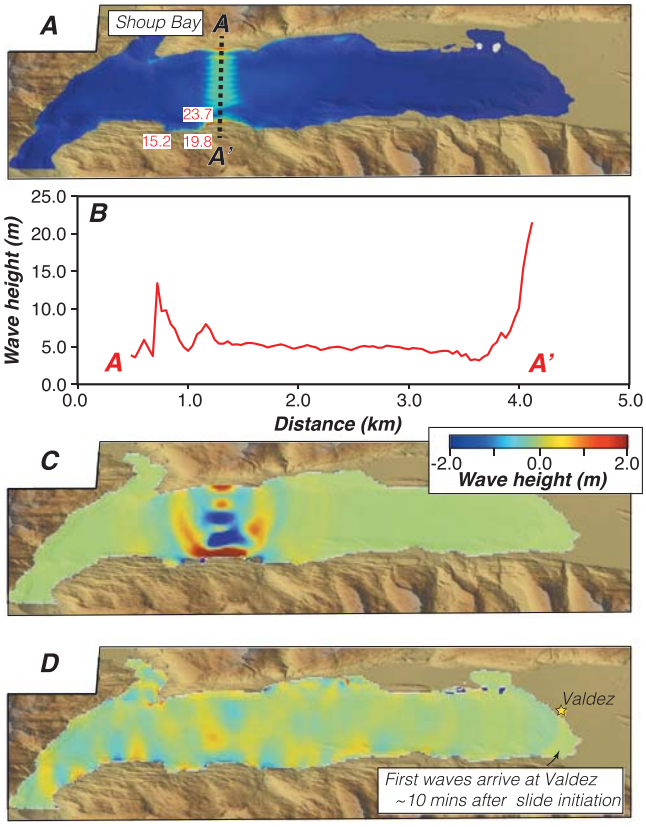

Figure 9. Results of hydrodynamic modeling of the Shoup Bay submarine landslide. (a) The maximum amplitude waves from 30 min of propagation are plotted. (b) A transect of wave height is shown that corresponds to the A-A' line in Figure 9a; wave height matches observations by *Plafker et al.* [1969]. (c) A snapshot at 2 min is shown with the color scale saturated to 2 m so that lower amplitude waves can be seen. (d) The first arrivals at Valdez old town are shown, after about 10 min propagation time.

3.2. Tsunami Modeling Results

We run the COULWAVE model to test whether our interpreted submarine landslide source model can explain observations at Valdez old town. We are thus primarily concerned with the backward propagating wave toward the Valdez site, which for a landslide source, begins with a depression or drawdown phase (Figure 8a). This is caused by initial excavation during landslide movement. The first positive, elevation phase of the back-going wave is generated in the region of deposition (Figures 8b–8d). The outgoing wave, propagating in the direction of slide movement and in deeper water, has the opposite polarity and quickly moves out to the west (Figure 8).

Preserved landslide deposits are also noted on the west end of Port Valdez fjord that broke off from the submerged terminal moraine at the end of Shoup Bay and slid out to the center of the fjord floor [*Lee et al.*, 2006, 2007; *Ryan et al.*, 2010] (Figure 4). Very high runups were noted on the west end of Port Valdez of up to 65 m [e.g., *Grantz et al.*, 1964; *Plafker et al.*, 1969] that were initially attributed to the delta-front slide [e.g., *Wilson and Tørum*, 1971], but it is more likely that they had a local source at Shoup Bay. To assess the effects of landslide tsunamis from the west end of the fjord at Valdez old town, we conduct a similar modeling exercise for the Shoup Bay slides as was described above for the delta slide. The modeled Shoup Bay tsunami source was shifted slightly to the east from its historic location to avoid spurious generation effects from the slide deposits in the present-day bathymetry. Because these slides happened 15–20 km from Valdez old town, we expect the effects to be far less important there than those from the delta slide [*Nicolsky et al.*, 2013]. Indeed, the amplitude of the wave height is an order of magnitude lower at Valdez Harbor (Figure 8g). Although, our modeling of the Shoup slide reproduces the runup values and directions measured by *Plafker et al.* [1969] across from Shoup Bay (20–23 m) (Figure 9), there is greater uncertainty associated with the source, owing to the difficulty in determining the preslide topography/bathymetry and partial subaerial origin.

3.3. Comparison to Observations

We compare modeled and observed wave height, inundation, and some limited resolution of current directions as related to the motions of the *S.S. Chena* to evaluate our simple submarine landslide scenario. Our modeled wave heights of the elevation wave are consistent with a Lowe River delta-front slide source to generate the tsunami at Valdez old town and match the lower end of the spectrum of eyewitness accounts at about 4.5 m, with the high end being 7.6 m [*Brown*, 1964]. Eyewitness accounts of wave height are understandably difficult to quantify and depend on different local objects used for scaling. A study examining eyewitness accounts of the 2004 Indian Ocean tsunami in Thailand found a 5–15 m aboveground-level range in reported tsunami height of the same wave, depending on the observer [*Mård Karlsson et al.*, 2009].

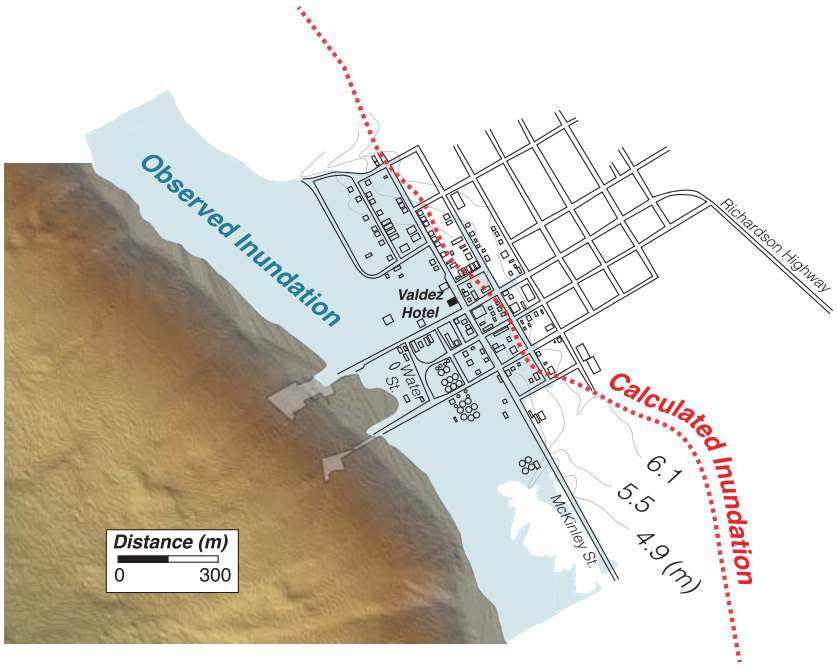

Figure 10. Comparison of observed tsunami inundation (blue shading) [*Wilson and Tørum*, 1971] in Valdez old town with calculated maximum inundation (red dashed line) from the delta-front slide source. Postearthquake elevation contours are shown that imply that the observed water height reached 6.1 m above mean sea level. The tsunami modeling used a smoother version of the topography to make calculations possible. However, a fairly close match between observed and calculated runup heights was achieved.

Perhaps, a better-quantified measure of the tsunami is maximum horizontal inundation distance, which in a developed environment can be measured using water level marks on structures. This assumes that the largest, initial wave is primarily responsible for maximum inundation, which is verified by *Coulter and Migliaccio* [1966], who report that the initial wave reached McKinley Street in Valdez old town (Figure 10). We compare a map made by *Wilson and Tørum* [1971] of maximum inundation with our calculated value and note very close agreement in many parts of Valdez old town, though overall, the calculated inundation is greater than observed. Given the input smoothed topography necessary to make the intensive hydrodynamic calculations, the agreement between calculated and observed inundation is quite close.

Another way to assess the tsunami modeling is to compare the flow directions and sequence against the observed timeline of events, in particular, the movements of the *S.S. Chena*. This may be the most diagnostic measure of the submarine landslide tsunami character, because the distance between the landslide excavation and deposition regions (along with slide velocity) controls the temporal separation between negative and positive tsunami phases. By most accounts [e.g., *Coulter and Migliaccio*, 1966; *Wilson and Tørum*, 1971] the first effect on the *Chena* was that it was pulled away from the collapsing north dock in Valdez old town in a northwesterly direction (Figure 2). This agrees well with the modeled initial negative wave that we calculate, which would have drawn the *Chena* to the northwest (Figure 8a). Very shortly thereafter (sometimes reported as simultaneously), people in town and on board the *Chena* say it was tossed up on a large incoming wave. We calculate that this happened less than a minute after the maximum drawdown (Figure 8b). Since the inner small boat harbor was walled off by the north and south piers/jetties, there was a delay in its filling, leaving the *Chena* temporarily aground. We then calculate that the initial positive wave flows east along the southeast trending shoreline, which is consistent with the *Chena*'s movements and the account of the captain, who said that the vessel was unable to resist the very strong, alongshore currents for some time (Figure 8c). Between 5 and 6 min after slide initiation our calculations show some return flow and a small drawdown below mean sea level (Figure 8e); this is about the time that the cascading of water over the landslide scarp was filmed on board the *Chena*.

Eyewitness accounts all mention a second, smaller wave striking Valdez old town about 10 min after the first that left the Valdez Hotel (see Figure 10 for location) with about 0.5 m of water in it. One possibility is that this wave resulted from slides at Shoup Bay, where preserved landslide deposits are imaged by multibeam bathymetry [*Lee et al*., 2006, 2007; *Ryan et al*., 2010] (Figures 4 and 9). Our modeling of the Shoup Bay slide does indicate a small wave (0.15 m) hitting Valdez old town after 11 min (10 min after the initial wave at Valdez; Figure 8g), which also coincides with a secondary phase (0.5 m high) from the delta-front slide (Figure 8f). The timing of these events corresponds with the observations, but the modeled amplitudes at old town are not as great as the reported 0.5 m of water inside of the Valdez Hotel which sat about 4 m above mean sea level (Figure 10), though it is unclear how much of the water from the initial waves had drained off at that point. *Nicolsky et al*. [2013] also have difficulty in modeling this second wave at 10 min using simultaneous delta-front and Shoup Bay tsunami sources.

We conclude that the failure mode we modeled for the delta front is consistent with observations of initial wave height, the observed inundation, and the timeline of events as reported by eyewitnesses. While additional failures of the east end of the fjord clearly occurred, we conclude that they did not contribute significantly to the primary tsunami that struck at Valdez old town.

4. Conclusions

We combine new geophysical data, interpretation of post-1964 bathymetric changes, and numerical modeling of submarine landslide-generated tsunamis to interpret the events on 27 March 1964 in Valdez. We use detailed hydrographic observations made in 1959 in the area adjacent to the harbor at Valdez old town, and depth measures made as part of multibeam surveys conducted in 2006 to build DEMs that when compared show that the primary failure of the delta front on the east end of Port Valdez fjord occurred just south of town, involving a ~1500 m long area that receded to the east by about 150 m.

We interpret high-resolution seismic reflection data as showing about 75 m of mostly unfailed sediment accumulation that is interrupted by relatively narrow chutes (≤400 m wide) where slide debris was transported. Hummocky deposits are preserved at the end of the primary chute (Figure 1) and likely represent blocky parts of the failed material. However, some of the materials must have mobilized more fully to flow out onto the deep fjord floor, leaving debris lobe deposits that have been mapped and sampled [*Lee et al*., 2007; *Ryan et al*., 2010]. Viscoplastic models of the debris flow [*Imran et al*., 2001] yield a complex time history of movement caused by the sharp change in slope and bilinear rheology. Displacement of the flow in the excavation region (steep slope) occurred very rapidly after the onset of failure and was primarily responsible for generating the tsunami. Results from nonlinear hydrodynamic modeling of this slide are consistent with the timeline of events at Valdez old town, eyewitness accounts of wave height, and measured inundation.

Acknowledgments
The authors appreciate two anonymous reviews and the efforts of Editor Andre Revil. USGS acquired data are available by contacting the corresponding author.

References

Arendt, A., K. Echelmeyer, W. Harrison, C. Lingle, S. Zirnheld, V. Valentine, B. Ritchie, and M. Druckenmiller (2006), Updated estimates of glacier volume changes in the western Chugach Mountains, Alaska, and a comparison of regional extrapolation methods, *J. Geophys. Res.*, *111*, F03019, doi:10.1029/2005JF000436.

Barclay, D. J., G. C. Wiles, and P. E. Calkin (2009), Holocene glacier fluctuations in Alaska, *Quat. Sci. Rev.*, *28*(21–22), 2034–2048, doi:10.1016/j.quascirev.2009.01.016.

Brown, D. L. (1964), Tsunamic activity accompanying the Alaskan earthquake of 27 March 1964, *Tech. Rep.*, 20 pp., U.S. Army Engineer District, U.S. Army Corps of Eng., Anchorage, Alaska.

Caldwell, R. J., B. W. Eakins, and E. Lim (2011), Digital elevation models of Prince William Sound, Alaska: Procedures, data sources and analysis, *NOAA Tech. Mem. NESDIS NGDC-40*, 47 pp., U.S. Dept. of Commer., Boulder, Colo.

Coulter, H. W., and R. R. Migliaccio (1966), Effects of the earthquake of March 27, 1964 at Valdez, Alaska, *U.S. Geol. Surv. Prof. Pap.*, 542-c, 36.

Dalla Valle, G., F. Gamberi, P. Rocchini, D. Minisini, A. Errera, L. Baglioni, and F. Trincardi (2013), 3D seismic geomorphology of mass transport complexes in a foredeep basin: Examples from the Pleistocene of the Central Adriatic Basin (Mediterranean Sea), *Sediment. Geol.*, *294*, 127–141.

Enet, F., and S. T. Grilli (2007), Experimental study of tsunami generation by three-dimensional rigid underwater landslides, *J. Waterw. Port Coastal Ocean Eng.*, *133*, 442–454.

Fernández-Nieto, E. D., F. Bouchut, D. Bresch, M. J. Castro Diaz, and A. Mangeney (2008), A new Savage-Hutter type model for submarine avalanches and generated tsunami, *J. Comput. Phys.*, *227*, 7720–7754.

Gales, J. A., P. T. Leat, R. D. Larter, G. Kuhn, C.-D. Hillenbrand, A. G. C. Graham, N. C. Mitchell, A. J. Tate, G. B. Buys, and W. Jokat (2014), Large-scale submarine landslides, channel and gully systems on the southern Weddell Sea margin, Antarctica, *Mar. Geol.*, *348*, 73–87.

Geist, E. L., P. J. Lynett, and J. D. Chaytor (2009), Hydrodynamic modeling of tsunamis from the Currituck landslide, *Mar. Geol.*, *264*, 41–52.

Grantz, A., G. Plafker, and R. Kachadoorian (1964), *Alaska's Good Friday Earthquake, March 27,1964. A Preliminary Geologic Evaluation*, Survey Circular, vol. 491, 44 pp., U.S. Geol. Surv., Washington, D. C.

Imran, J., P. Harff, and G. Parker (2001), A numerical model of submarine debris flow with graphical user interface, *Comput. Geosci.*, *27*, 717–729.

Jiang, L., and P. H. Leblond (1994), Three-dimensional modeling of tsunami generation due to a submarine mudslide, *J. Phys. Oceanogr.*, *24*, 559–572.

Jintasaeraneea, P., W. Weinrebea, I. Klauckea, A. Snidvongsb, and E. R. Flueh (2012), Morphology of the Andaman outer shelf and upper slope of the Thai exclusive economic zone, *J. Asian Earth Sci.*, *46*, 78–85.

Kennedy, A. B., Q. Chen, J. T. Kirby, and R. A. Dalrymple (2000), Boussinesq modeling of wave transformation, breaking and runup: I. One dimension, *J. Waterw. Port Coastal Ocean Eng.*, *126*, 39–47.

Laberg, J. S., K. Kawamura, H. Amundsen, N. Baeten, M. Forwick, T. A. Rydningen, and T. O. Vorren (2014), A submarine landslide complex affecting the Jan Mayen Ridge, Norwegian-Greenland Sea: Slide-scar morphology and processes of sediment evacuation, *Geo Mar. Lett.*, *34*, 51–58, doi:10.1007/s00367-013-0345-z.

Lastras, G., et al. (2013), Landslides cause tsunami waves: Insights from Aysén Fjord, Chile, *Eos Trans. AGU*, *94*, 297–298, doi:10.1002/2013EO340002.

Lee, H., H. F. Ryan, R. E. Kayen, P. J. Haeussler, P. Dartnell, and M. A. Hampton (2006), Varieties of submarine failure morphologies of seismically-induced landslides in Alaskan fjords, *Norw. J. Geol.*, *86*, 221–230.

Lee, H. J., H. F. Ryan, P. J. Haeussler, R. E. Kayen, M. A. Hampton, J. Locat, E. Suleimani, and C. R. Alexander (2007), Reassessment of seismically induced, tsunamigenic submarine slope failures in Port Valdez, Alaska, USA, in *Submarine Mass Movements and their Consequences*, edited by V. Lycousis, D. Sakellarion, and J. Locat, pp. 357–365, Springer, Dordrecht, Netherlands.

Locat, J. (1997), Normalized rheological behaviour of fine muds and their flow properties in a pseudoplastic regime, in *Debris-Flow Hazard Mitigation: Mechanics, Prediction, and Assessment, Proceedings of First International Conference*, edited by C.-L. Chen, pp. 260–269, Water Resour. Div., Am. Soc. of Civil Eng., New York.

Locat, J., H. J. Lee, P. Locat, and J. Imran (2004), Numerical analysis of the mobility of the Palos Verdes debris avalanche, California, and its implication for the generation of tsunamis, *Mar. Geol.*, *203*, 269–280.

Locat, J., H. Lee, U. ten Brink, D. C. Twichell, E. L. Geist, and M. Sansoucy (2009), Geomorphology, stability and mobility of the Currituck slide, *Mar. Geol.*, *264*, 28–40.

Lynett, P., and P. L. F. Liu (2001), Submarine landslide generated waves modeled using depth-integrated equations, in *Submarine Landslides and Tsunamis*, edited by A. C. Yalciner et al., pp. 51–58, Kluwer Acad., Dordrecht, Netherlands.

Lynett, P., and P. L. F. Liu (2002), A numerical study of submarine-landslide-generated waves and run-up, *Proc. R. Soc. London, Ser. A*, *458*, 2885–2910.

Lynett, P. J. (2006), Nearshore wave modeling with high-order Boussinesq-type equations, *ASCE J. Waterw. Harbors Div.*, *132*, 348–357.

Lynett, P. J., and P. L.-F. Liu (2005), A numerical study of run-up generated by three-dimensional landslides, *J. Geophys. Res.*, *10*, C03006, doi:10.1029/2004JC002443.

Lynett, P. J., T.-R. Wu, and P. L.-F. Liu (2002), Modeling wave runup with depth-integrated equations, *Coastal Eng.*, *46*, 89–107.

Mård Karlsson, J., A. Skelton, M. Sandén, M. Ioualalen, N. Kaewbanjak, N. Pophet, J. Asavanant, and A. von Matern (2009), Reconstructions of the coastal impact of the 2004 Indian Ocean tsunami in the Khao Lak area, Thailand, *J. Geophys. Res.*, *114*, C10023, doi:10.1029/2009JC005516.

Masson, D. G., C. B. Harbitz, R. B. Wynn, G. Pedersen, and F. Løvholt (2006), Submarine landslides: Processes, triggers and hazard prediction, *Philos. Trans. R. Soc. A*, *364*, 2009–2039.

Migeon, S., A. Cattaneo, V. Hassoun, C. Larroque, N. Corradi, F. Fanucci, A. Dano, B. Mercier de Lepinay, F. Sage, and C. Gorini (2011), Morphology, distribution and origin of recent submarine landslides of the Ligurian Margin (North-western Mediterranean): Some insights into geohazard assessment, *Mar. Geophys. Res.*, *32*, 225–243, doi:10.1007/s11001-011-9123-3.

Nicolsky, D. J., E. N. Suleimani, P. J. Haeussler, H. F. Ryan, R. D. Koehler, R. A. Combellick, and R. A. Hansen (2013), Tsunami Inundation Maps of Port Valdez, Alaska, *Report of Investigations 2013-1*, 85 pp., State of Alaska Dep. of Nat. Resour., Div. of Geol. and Geophys. Surv., Fairbanks.

Park, H., D. T. Cox, P. J. Lynett, D. M. Wiebe, and S. Shin (2013), Tsunami inundation modeling in constructed environments: A physical and numerical comparison of free-surface elevation, velocity, and momentum flux, *Coastal Eng.*, *79*, 9–21.

Plafker, G., R. Kachadoorian, E. B. Eckel, and L. R. Mayo (1969), Effects of the earthquake of March 27, 1964 on various communities, *U.S. Geol. Surv. Prof. Pap.*, 542-G, 50.

Ritter, H. P. (1901), Descriptive report to accompany, Hydrographic Sheet No. 2554, 12 pp.

Ryan, H. F., H. J. Lee, P. J. Haeussler, C. R. Alexander, and R. E. Kayen (2010), *Submarine Mass Movements and Their Consequences*, Advances in Natural and Technological Hazards Research, vol. 28, edited by D. C. Mosher et al., pp. 411–421, Springer, Dordrecht, Netherlands.

Schwab, W. C., H. J. Lee, D. C. Twichell, J. Locat, C. H. Nelson, W. G. McArthur, and N. H. Kenyon (1996), Sediment mass-flow processes on a depositional lobe, outer Mississippi fan, *J. Sediment. Res.*, *66*, 916–927.

Seaborg, H. J. (1959), Hydrographic survey, Port Valdez, Prince William Sound, Alaska, U. S. Coast and Geodetic Survey, H-8493, B0-025159, 20 pp., Dep. of Commerce.

Suleimani, E., D. J. Nicolsky, P. J. Haeussler, and R. Hansen (2011), Combined effects of tectonic and landslide-generated tsunami runup at Seward, Alaska during the *Mw* 9.2 1964 earthquake, *Pure Appl. Geophys.*, *168*, 1053–1074.

Tappin, D. R. (2010), Digital elevation models in the marine domain: Investigating the offshore tsunami hazard from submarine landslides, *Geol. Soc. London Spec. Publ.*, *345*, 81–101, doi:10.1144/SP345.10.

ten Brink, U. S., H. J. Lee, E. L. Geist, and D. Twichell (2009), Assessment of tsunami hazard to the U.S. East coast using relationships between submarine landslides and earthquakes, *Mar. Geol.*, *264*, 65–73.

Twichell, D. C., J. D. Chaytor, U. S. ten Brink, and B. Buczkowski (2009), Morphology of late Quaternary submarine landslides along the U.S. Atlantic continental margin, *Mar. Geol.*, *264*, 4–15.

Ward, S. N. (2001), Landslide tsunami, *J. Geophys. Res.*, *106*, 11,201–11,215, doi:10.1029/2000JB900450.

Wilson, B. W., and A. Tørum (1971), Effects of the tsunamis: An engineering study, in *The Great Alaska Earthquake of 1964: Oceanography and Coastal Engineering*, pp. 361–523, Natl. Acad. of Sci., Washington, D. C.

World Glacier Monitoring Service (2008), *Global Glacier Changes: Facts and Figures*, edited by M. Zemp et al., 88 pp., UNEP, World Glacier Monitoring Service, Zurich, Switzerland.